



Anti-pollution polyethersulfone/sulfonated polysulfone (PES/SPSf) membrane with different sulfonation degree by reverse thermally induced phase separation (RTIPS) procedure

Hang Yang^a, Chun-Mei Gao^{a,b,c}, Sheng-Hui Liu^{a,c,*}, Shi-Feng Ji^{a,c}, Hong-Yu Chen^a, Jin-Chao Chen^a

^aCollege of Marine Ecology and Environment, Shanghai Ocean University, Shanghai, China, Tel. +86 18317052279/86 2161900330; Fax: 86 2161908337; email: shliu@shou.edu.cn (S.-H. Liu), Tel. +86 18721052291; email: 466215962@qq.com (H. Yang), Tel. +86 15692165063; email: cmgao@shou.edu.cn (C.-M. Gao), Tel. +86 18616551176; email: sfji@shou.edu.cn (S.-F. Ji), Tel. +86 18616371207; email: 857282716@qq.com (H.-Y. Chen), Tel. +86 17835403451; email: 13605724249@163.com (J.-C. Chen)

^bCenter for Polar Research, Shanghai Ocean University, Shanghai, China

^cMarine Environment Monitoring and Assessment Center, Shanghai Ocean University, Shanghai, China

Received 1 January 2020; Accepted 2 May 2020

ABSTRACT

Polyethersulfone/sulfonated polysulfone (PES/SPSf) microfiltration (MF) membranes were fabricated via reverse thermally induced phase separation (RTIPS) method and non-solvent induced phase separation (NIPS) method using *N,N*-dimethyl acetamide (DMAc) and diethylene glycol (DEG) as solvent and non-solvent, respectively. Attenuated total reflectance Fourier transform-infrared (ATR-FTIR) revealed that SPSf was successfully blended with PES in PES/DMAc/DEG solution system. Membranes with completely sponge-like morphology and uniform porous top surface were prepared by RTIPS method, while dense skin surface and finger-like structure presented in the membranes by NIPS method. In addition, pure water flux and bovine serum albumin (BSA) rejection rate of most membranes fabricated via RTIPS method were higher than that of NIPS method. As for membranes prepared by RTIPS method, pure water flux first increased from 511 to 2,119 L/m² h and then decreased to 1,499 and 1,896 L/m² h, simultaneously, when the pure water flux reached 2,119 L/m² h, the BSA rejection rate could still kept at a high level (70.11%). Furthermore, the water flux recovery ratio of membranes containing SPSf were much higher (>80%) than that of the pure PES membrane (59.21%). These results indicated that the permeability and anti-pollution performance of the PES/SPSf membrane could be enhanced with increasing sulfonation degree of SPSf, moreover, RTIPS method was a superior method for membrane preparation.

Keywords: Reverse thermally induced phase separation (RTIPS) method; Hydrophilicity; Sulfonated polysulfone (SPSf); Sulfonation degree

1. Introduction

Polyethersulfone (PES) is widely used in membrane preparation field due to its good mechanical strength, excellent acidic, and alkaline resistance and its high glass transition temperature [1–3]. However, the strong hydrophobicity

results in severe membrane fouling and greatly reduction of the polyethersulfone membrane service life, which limits its wide application in water treatment field. Therefore, many strategies have been taken to enhance the hydrophilicity of PES membrane to improve anti-fouling performance [4–6]. The most effective and feasible method is blending owing to its convenient operations and mild conditions.

* Corresponding author.

The polymer blending modification is to mix the hydrophilic polymer with the hydrophobic polymer in a specific weight ratio, thereby improving the hydrophilicity of the membrane [1,7]. Quantities of studies have proved that due to the existence of hydrophilic substances such as oxidized multi-walled carbon nanotubes (O-MWCNTs) [8], CuO [9], cellulose acetate [10], and so on in hydrophobic polymer membranes, thus, the membranes with better hydrophilicity, antifouling performance, and water permeability are successfully prepared. Gumbi et al. [8] introduced O-MWCNTs nanoparticles to dimethylacetamide/polyethylene glycol/Polyethersulfone/sulfonated polysulfone (DMAc/PEG/PES/SPSf) casting solution and successfully prepared membranes with sponge-like structure, excellent water permeability with almost unchanged retentions, hydrophilicity, mechanical strength, and fantastic antifouling ability. However, the compatibility of polymers is a key factor affecting the composition of the casting solution, which further affects the membrane performance. Therefore, it is very important to select or synthesize hydrophilic additives in which the properties are similar to the membrane non-ionic materials such as SPSf [11,12] and sulfonated polyethersulfone (SPES) [13]. SPSf is chosen to be blended with PES to produce membranes with excellent properties due to the similarity of chemical structure and properties between SPSf and PES. Li et al. [1] proved that PES and SPSf polymers showed a very good miscibility, and the PES/SPSf membrane with outstanding water permeability and antifouling ability, however, the PES/SPSf membranes prepared by non-solvent induced phase separation (NIPS) method, finger structure has appeared inevitably. Therefore, in order to obtain membranes with good properties, it is necessary to develop a new method to prepare membrane materials.

Simultaneously, the preparation method has a great influence on membrane structure and properties. Phase inversion method, which is often used to fabricate commercial polymeric membranes such as microfiltration (MF) and ultrafiltration (UF), including non-solvent induced phase separation (NIPS) method and thermally induced phase separation (TIPS) process. During the NIPS process, the solvent and nonsolvent exchange rapidly, which is more conducive to the formation of dense skin layer and finger-like structure [14], this phenomenon limits the wide application of NIPS method in membrane preparation. Therefore, the upper critical solution temperature (UCST)-TIPS process was invented by Castro [15]. Although it is critical to improve the defects of the membranes by NIPS method, higher preparation temperatures and less volatile diluents hinder the widespread of TIPS process. Though many studies had been reported the improved TIPS process [16–18], this mechanism still could not solve the problem of high energy consumption. As a new membrane preparation technology, the lower critical solution temperature (LCST)-TIPS (reverse TIPS, i.e., RTIPS) process which was proposed by Liu et al. [19], has received unprecedented attention due to the combination of the advantages between NIPS and TIPS process. The PES membranes with the bi-continuous structure were attained via RTIPS method, which showed a higher pure water permeation flux and excellent mechanical properties than that of membranes prepared by NIPS process.

The aim of this study is to improve the hydrophilicity and anti-fouling property of PES-based blend membrane by investigating the effect of sulfonation degree of SPSf and membrane preparation mechanism on compatibility, morphologies, and properties of the PES/SPSf membrane. To achieve this, the PES/SPSf membrane was prepared with different sulfonation degree of SPSf via RTIPS method. The performance of PES/SPSf membrane was studied by pure water flux, bovine serum albumin (BSA) rejection rate and BSA flux variation in a long time. The thermal stability of membranes was determined by thermogravimetric analysis (TGA). The surface morphology and cross-sectional structures were recorded by scanning electron microscopy (SEM) while the surface roughness and hydrophilicity were measured using atomic force microscopy (AFM) and water contact angle, respectively. Compared with other flat-sheet membranes, the advantages of membranes prepared in this work were also observed.

2. Experimental

2.1. Materials

PES ($M_w = 45,000$) and polysulfone (PSF) were purchased from BASF (Germany) and Shandong Jinlan Special Polymer Co., Ltd., (China), respectively. Sodium hydroxide (NaOH), dichloroethane ($C_2H_4Cl_2$), oleum (H_2SO_4), and phenolphthalein obtained from Shanghai Chemical Agent Co., Ltd., (China). The materials were placed in the drying oven at $60^\circ C$ for 1 d before using. DMAc and diethylene glycol (DEG) were supplied by Sinopharm Chemical Reagent Co., Ltd., BSA ($M_w = 67,000$) was obtained from Shanghai Liangan Biochemical Engineering Co., Ltd. Pure water was self-made.

2.2. Preparation of SPSf

Fifty milliliters of $C_2H_4Cl_2$ and 10 g of PSF were added into a three-necked flask equipped with a stirrer, a dropping funnel, an air condenser, and a thermometer. After stirring and dissolving uniformly, oleum was added slowly. With the addition of oleum, the reactants were changed from clear to mixed, and then occurred phase separation. After the reaction was complete, $C_2H_4Cl_2$ and excess acid were poured out, then washed with distilled water to neutrality, and dried in a $50^\circ C$ vacuum drying oven to obtain the SPSf.

The method for measuring the degree of sulfonation was as follows: 0.3 g SPSf and 30 mL of a 1 mol/L NaCl solution were placed in a sample tube and shaken repeatedly. After an overnight rest, 10 mL of the solution was titrated with 0.05 mol/L of NaOH solution in the presence of phenolphthalein as an indicator.

$$IEC = \frac{3NV}{W} \quad (1)$$

$$DS = \left(\frac{IEC \times 442}{1,000} \right) \times 100\% \quad (2)$$

where N is the equivalent concentration of sodium hydroxide standard solution, V is the volume of consumed sodium hydroxide standard solution, W is the quality of SPSf.

2.3. PES/SPSf membrane preparation

The blend membranes were fabricated via reverse thermally induced phase separation (RTIPS) method. Table 1 shows the components of the casting solution for the PES/SPSf membrane fabrication. DMAc and DEG were added into an Erlenmeyer flask, then SPSf with different sulfonation degree (0%, 5%, 10%, 15%, 20%, and 25%) was dissolved in mixed solvents, and weighed amounts of PES were dispersed into cast solution and stirred about 24 h at room temperature. The prepared cast solution was left at room temperature for 24 h to remove the bubbles. After degasification, the solution was cast on a smooth glass plate with a scraper gap of 300 μm and quickly immersed in the coagulation water bath with different temperature (Table 2) for phase separation, the schematic diagram of the PES/SPSf membrane preparation process by RTIPS method and NIPS method is illustrated in Fig. 1.

2.4. Membrane characterization

The light transmittance experiment was used to study what was the main driving force during the phase separation process. The method and device were first reported by Li et al. [20]. The phase separation rate of the casting solution was characterized by the relationship between the light transmittance intensity through the recording membrane and the immersion time.

The viscosity of the PES/SPSf cast solution was measured by DV-II+PRO Digital Viscometer (Brookfield, USA) at 25°C.

The cloud point was determined by a self-made device [21], the testing process was as follows: transparent homogeneous casting solution was poured into a sealed tube, and then heated evenly from 25°C to 70°C at a rate of 1°C/min in a water bath. When the turbidity of the casting solution occurred, the temperature was the cloud point (i.e., LCST).

The thermal stability of the PES/SPSf membrane was measured via TGA (TGA1000C, China) from 20°C to 1,000°C at a heating rate of 20°C/min under nitrogen atmosphere.

The digital micrometer was used to determine the thickness of wet membranes. The dry-wet weight method was used to measure membrane porosity [22]. First, gently

wiped the surface moisture of the wet membrane samples with a filter paper and weighed it. The wet membrane samples were then dried in vacuum condition (60°C) until the water completely evaporated. Porosity was calculated by Eq. (3):

$$\varepsilon = \frac{(W_1 - W_2) / \rho_1}{(W_1 - W_2) / \rho_1 + W_2 / \rho_2} \times 100\% \quad (3)$$

where ε is the porosity of membrane, W_1 is the wet sample weight (g), W_2 is the dry sample weight (g), ρ_1 and ρ_2 are the density of pure water (1 g cm³) and PES (1.370 g cm³).

The average pore size (r_m) of PES/SPSf blend membrane was determined by the formula of Guerout-Elford-Ferry [23]:

$$r_m = \sqrt{\frac{(2.9 - 1.75\varepsilon) \times 8\eta h Q}{\varepsilon \times A \times \Delta P}} \quad (4)$$

where r_m is the average pore size (μm), ε is the porosity of membrane, η is the water viscosity (8.9×10^{-4} Pa/s), h is the membrane thickness (mm), Q is pure water transmittance (mL/s), A and ΔP are the membrane area (cm²) and feed pressure (0.1 MPa), respectively.

The maximum pore size (r_{max}) of the membrane was calculated using the bubble point method according to Laplace's law [24]:

Table 2
Coagulation water bath temperature

Membrane number	Water bath temperature (°C)
MSPSf-0-25	25
MSPSf-0-60	60
MSPSf-5-60	60
MSPSf-10-60	60
MSPSf-15-25	25
MSPSf-15-60	60
MSPSf-20-60	60
MSPSf-25-60	60

Table 1
Components of the cast solution

Membrane no.	Cast solution composition (wt.%)				Sulfonation degree of SPSf (%)
	DMAc	DEG	PES	SPSf	
MSPSf-0	46.1	36.9	17	0	0
MSPSf-5	46.1	36.9	15	2	5
MSPSf-10	46.1	36.9	15	2	10
MSPSf-15	46.1	36.9	15	2	15
MSPSf-20	46.1	36.9	15	2	20
MSPSf-25	46.1	36.9	15	2	25

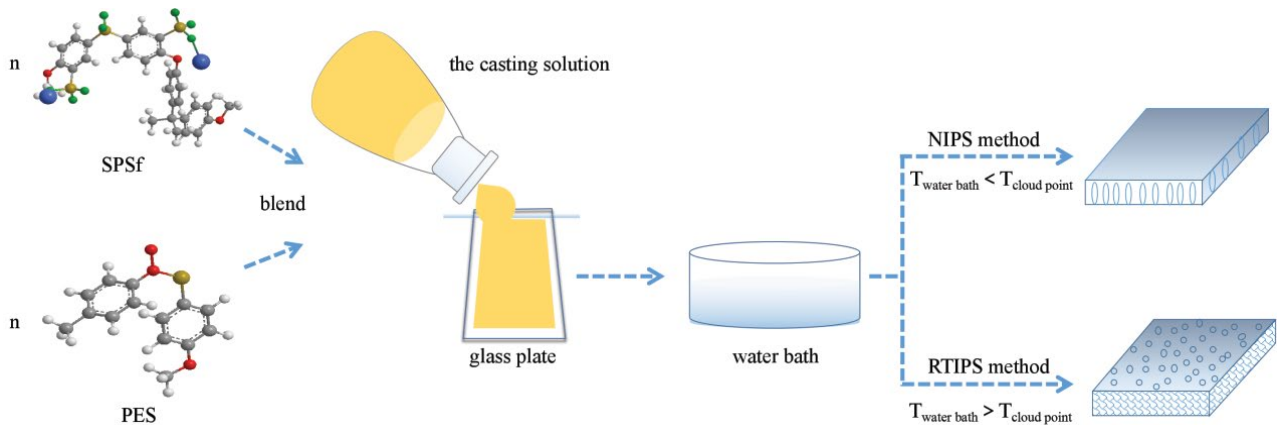


Fig. 1. Schematic diagram of PES/SPSf membrane preparation process.

$$r_{\max} = \frac{2\sigma \cos\theta}{P} \quad (5)$$

where σ , θ , and P are the surface tension of water (22.8×10^{-3} N/m), the membrane contact angle ($^\circ$) and minimum bubble point pressure (MPa), respectively.

The surface and cross-sectional morphologies of PES/SPSf membrane were studied by SEM (S-3400II, Hitachi High-Technologies, Japan). The cross-section of the membrane was obtained by freeze-breaking in liquid nitrogen. All samples were cut into small squares (approximately 1 cm^2) and glued onto a special stage followed by spraying with gold.

The roughness of the flat-sheet membrane was investigated by AFM (Veeco, Nanoscope IIIa Multimode AFM). The scanning area of the membrane was $20 \mu\text{m} \times 20 \mu\text{m}$. The roughness was analyzed by NanoScope analysis software, the 3D AFM image was drawn by Gwyddion software.

Attenuated total reflectance Fourier transform-infrared (ATR-FTIR) spectrometer (Nicolet 6700, Thermo Electron Scientific Instruments Corp.) to characterize functional groups of the PES/SPSf membrane. The hydrophilicity of the PES/SPSf membrane was evaluated by a contact angle goniometer (JC2000A, Shanghai Zhongcheng Digital Equipment Co., Ltd., China) according to the process as follows: approximately $5 \mu\text{L}$ of water droplets were dropped on the dried membrane surface, and then images were taken with a camera to determine the water contact angle. In order to reduce the error, the contact angle was measured at least three times and then averaged.

2.5. Membrane performance tests

The testing system for pure water flux (J_w) and BSA (300 mg L^{-1}) rejection rate (R) was a self-made cross-flow filter. The membrane modules were continuously pre-pressed for 30 min at 0.1 MPa before testing. The BSA concentration in the feed and permeate solution was determined by UV (HACH, DR6000, USA) spectrophotometer at 280 nm. J_w and R could be calculated using Eqs. (4) and (5), respectively [25].

$$J_w = \frac{Q}{A \times t} \quad (6)$$

$$R(\%) = \left(1 - \frac{C_p}{C_f}\right) \times 100 \quad (7)$$

where Q is the volume of permeate (L), A is the membrane area (m^2), t is the operation hours (h), C_p and C_f are BSA concentrations in the permeate and feed solution, respectively.

After filtration of BSA solution, the fouled membrane was backwashed with alkali solution ($\text{pH} = 10$) for 30 min without pressure conditions, then the feed solution was replaced to pure water. The overall fouling process included three pure water filtration stages (J_w , J_{w1} and J_{w2}), two cleaning stages and two fouling stages. The variety of pure water flux and BSA of membrane with time was also tested, respectively. The water flux recovery rate $\text{FRR}(\%)$ could be calculated using the following equation:

$$\text{FRR}(\%) = \frac{J_{w2}}{J_w} \times 100 \quad (8)$$

3. Results and discussion

3.1. Synthetic pathway, sulfonation degree, and FTIR of SPSf

Figs. 2 and 3 display the synthetic pathway and FTIR spectrum of SPSf, respectively. The sulfonation degree of the prepared SPSf was calculated to be 5%, 10%, 15%, 20%, and 25%. The absorption peak at $1,102.60\text{--}1,233.74 \text{ cm}^{-1}$ represents the symmetrical stretching vibrations of $\text{O}=\text{S}=\text{O}$ in sulfuric group. The absorption peak at $2,359.21 \text{ cm}^{-1}$ represents the stretching vibrations of $-\text{S}-$ in sulfuric group. These results illustrate that sulfuric group was successful synthesized in SPSf.

3.2. Cloud point and viscosity

The cloud point values of the cast solution obtained by heating the cast solution from 25°C to 70°C at $1^\circ\text{C}/\text{min}$ are shown in Fig. 4, in which the cloud point of MSPSf-0, MSPSf-5, MSPSf-10, MSPSf-15, MSPSf-20, and MSPSf-25 are 43°C , 46°C , 48°C , 49°C , 50°C , and 50°C , respectively. In spite of the incompatibility between SPSf, PES, and DEG, DMAc/DEG/PES/SPSf system has good compatibility and

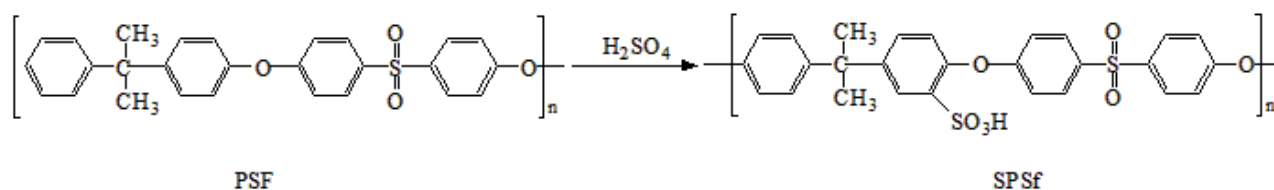


Fig. 2. Synthetic pathway of SPSf.

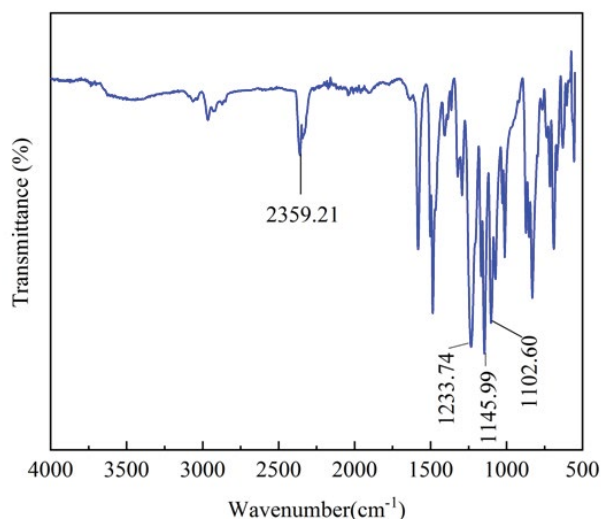


Fig. 3. FTIR spectra of SPSf.

outstanding stability [11]. The cloud points increase with increasing SPSf sulfonation degree, this can be explained by increasing hydrogen bonding. SPSf molecules are presented among the polymer chains and enhanced the interaction between the polymer chains and organic solvents, resulting in an increased cloud point. However, due to the good compatibility and outstanding stability of DMAc/DEG/PES/SPSf system at room temperature, as the sulfonation degree of SPSf increases, the hydrogen bonding is formed not anymore, so the growth rate of cloud point has slowed down.

The viscosities of different cast solution are shown in Fig. 4. When the sulfonation degree of SPSf increases from 0% to 25%, the initial viscosity of DMAc/DEG/PES/SPSf casting solution has improved. This phenomenon can be linked with increasing inter and intra-molecular hydrogen bonding interaction between PES and SPSf, which restrict the mobility of polymer chains due to the continuous addition of sulfonic acid groups ($-\text{SO}_3\text{H}$) [26]. However, as the sulfonation degree of SPSf increases, the growth rate of viscosity has slowed down. Since the fixed content of PES and excellent compatibility between PES/SPSf and mixed solvent (DMAc/DEG) at room temperature, hydrogen bonding is gradually saturated.

3.3. Light transmittance

Light transmittance curves, as shown in Fig. 5, illustrate a sharp drop at the beginning and then turn slowly until tend to flat. As for MSPSf-0–25 and MSPSf-15–25, the light transmittance of MSPSf-15–25 changes more slowly than

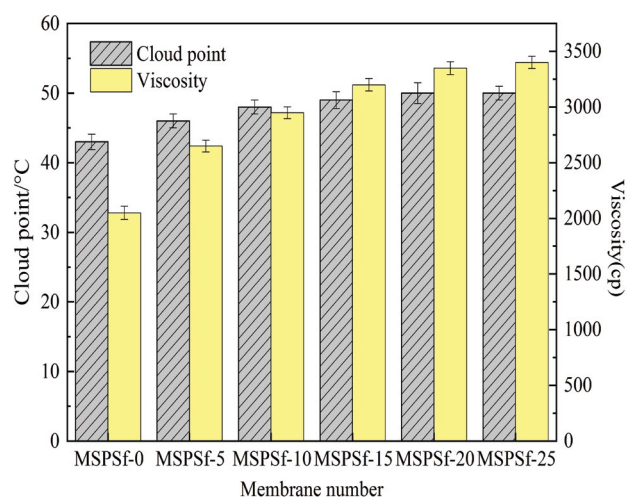


Fig. 4. Cloud point and viscosity of the cast solution with increasing sulfonation degree of SPSf.

that of MSPSf-0–25. This is because water bath temperature was lower than cloud point and the dominant principle was NIPS method based on mass transfer (Fig. 1), the MSPSf-15–25 has a high viscosity, which means slow mass transfer.

When the water bath temperature (60°C) was higher than the cloud point, the dominating membrane formation process was RTIPS mechanism based on heat transfer. The slope of the beginning part of the light transmittance curve for MSPSf-15–60 and MSPSf-25–60 decreases rapidly than that of MSPSf-0–60 and there is a little slope difference between MSPSf-15–60 and MSPSf-25–60. This result indicated that the phase separation rate of heat transfer and the viscosity are unrelated. Simultaneously, this further explains that the function of hydrophilic groups ($-\text{SO}_3\text{H}$) is greater than that of viscosity and the temperature gap value [27], then accelerates phase separation speed though generally high viscosity and a few differences of temperature gap will delay separation rate.

3.4. ATR-FTIR analysis of the PES/SPSf membrane

As shown in Fig. 6, ATR-FTIR spectra is often used to analyze organic functional groups. The absorption peak at $1,102.60\text{--}1,233.74\text{ cm}^{-1}$ represents the symmetrical stretching vibrations of S=O in sulfuric group [28]. In addition, the absorption peak at $2,359.21\text{ cm}^{-1}$ represents the stretching vibrations of $-\text{S}-$ in sulfuric group, which has no appearance in the spectrum of pure PES membrane (MSPSf-0–60). These results indicate that sulfuric group interacted with pure PES membrane successfully.

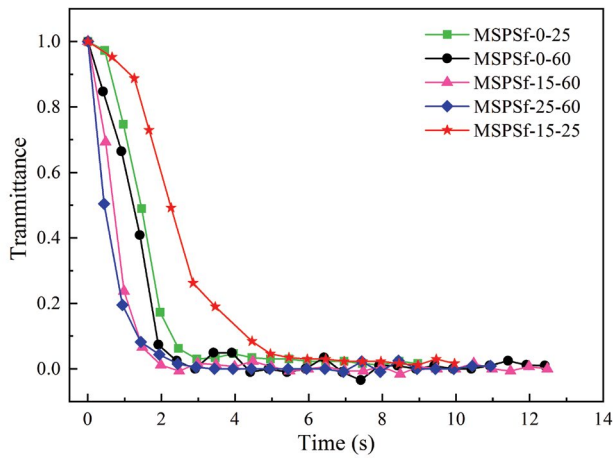


Fig. 5. Light transmittance curves of the cast solution.

3.5. Morphological studies

As mentioned before, NIPS and RTIPS method depended on the relationship between the cloud point of the membrane and the water bath temperature. The cloud point of MSPSF-15 is 49°C, it can be seen from Fig. 7 that the MSPSF-15–25 membrane, the coagulation water bath temperature (25°C) is lower than the cloud point, exhibiting a dense skin layer with only a few holes and asymmetric finger-like structure run through the whole cross-section. This is due to the direct contact of the membrane with water bath for instantaneous phase separation. However, as for MSPSF-15–60, the water bath temperature (60°C) is higher than cloud point, presenting sponge-like cross-section and homogeneous porous top surface, which is the evidence of high flux and outstanding BSA rejection rate shown in Fig. 12. Therefore, the mechanism of RTIPS is a better method for membrane preparation in phase-inversion method.

However, membrane structure and performance are affected by many factors, in order to further investigate the

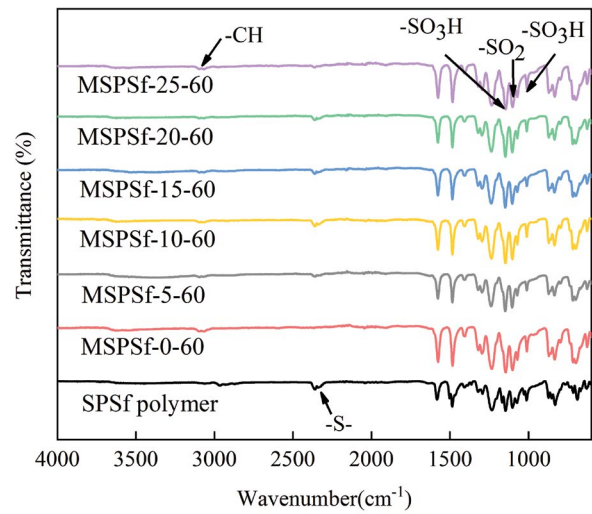


Fig. 6. ATR-FTIR spectra of the PES/SPSf membrane.

effect of sulfonation degree of SPSf, all membranes are prepared by RTIPS process. It can be seen from MSPSF-0–60 to MSPSF-25–60 that homogeneous porous surface is exhibited in Fig. 8. The number of pores increases first and then decreases a little with increasing sulfonation degree of SPSf and the highest porosity and maximum pore size are obtained at MSPSF-15–60. This phenomenon corresponds to pore size in Table 3. Additionally, SEM images of MSPSF-0–60 have a dense cross-section, as shown in Fig. 8, which indicates a rapid exchange rate owing to the main driving force of phase separation is heat transfer. Interestingly, the cross-sections of MSPSF-5–60 and MSPSF-10–60 present a conical-like structure in the supporting layer but this structure disappears in MSPSF-15–60, MSPSF-20–60, and MSPSF-25–60. The reason for this phenomenon is that more heat is needed to destroy the crosslinking structures between sulfonic acid groups and PES chains [29], which slows down the phase separation rate. Therefore, from MSPSF-0–60-c to MSPSF-25–60-c, it can be

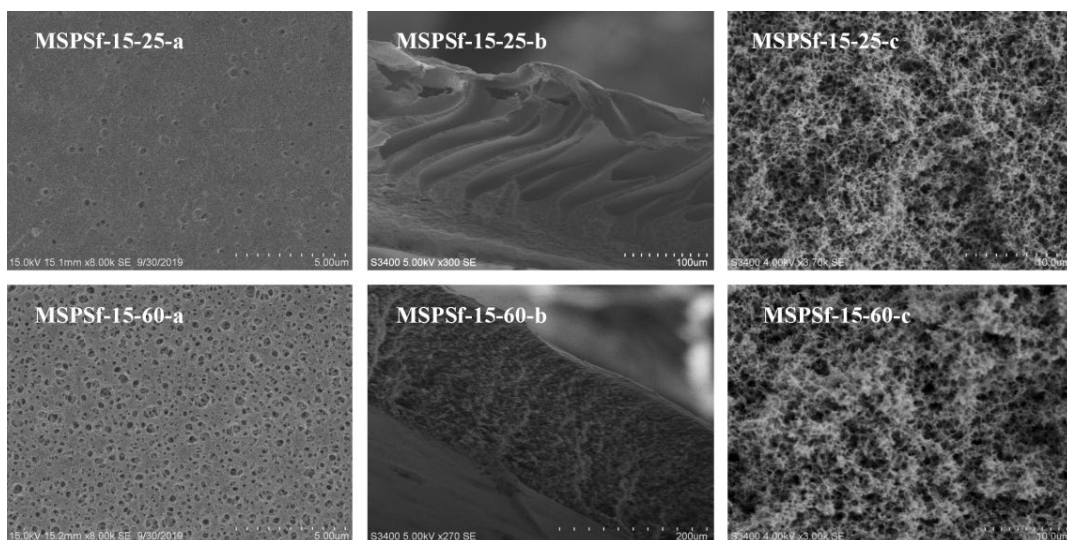


Fig. 7. SEM images of MSPSF-15 by NIPS and RTIPS.

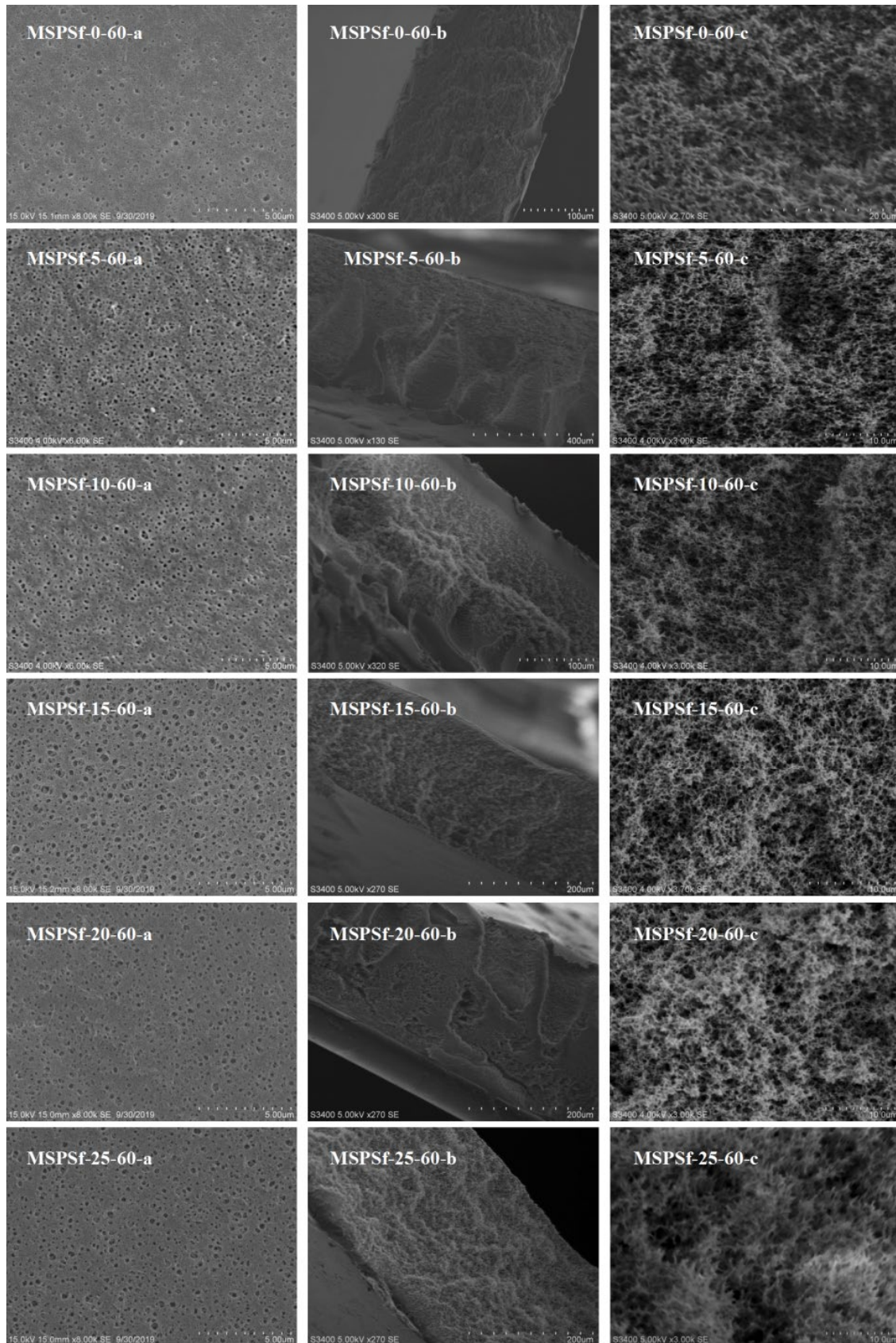


Fig. 8. SEM images of the membranes with different sulfonation degree of SPSf. (a) Enlarged top surface, (b) full cross-section, and (c) enlarged cross-section.

Table 3
Bulk porosity and pore size of membranes

Membrane number	Water bath temperature (°C)	Sulfonation degree of SPSf (%)	Bulk porosity (%)	r_m (μm)	r_{max} (μm)
MSPSf-0–25	25	0	78.0 ± 0.3	0.054 ± 0.002	0.237 ± 0.031
MSPSf-0–60	60	0	79.4 ± 0.1	0.062 ± 0.001	0.394 ± 0.005
MSPSf-5–60	60	5	83.4 ± 0.2	0.134 ± 0.003	0.323 ± 0.029
MSPSf-10–60	60	10	84.8 ± 0.2	0.159 ± 0.003	0.723 ± 0.026
MSPSf-15–25	25	15	85.3 ± 0.5	0.090 ± 0.002	0.432 ± 0.031
MSPSf-15–60	60	15	88.1 ± 0.2	0.176 ± 0.004	0.782 ± 0.008
MSPSf-20–60	60	20	84.1 ± 0.1	0.168 ± 0.001	0.698 ± 0.025
MSPSf-25–60	60	25	86.7 ± 0.4	0.154 ± 0.006	0.711 ± 0.011

seen more clearly that the cross-section changes from dense structure to sponge-like structure.

The AFM images of membranes with different sulfonation degree are displayed in Fig. 9. It shows that the surface roughness values of all the PES/SPSf membrane are higher than that of initial PES membrane. The Ra of MSPSf-0–60, MSPSf-5–60, MSPSf-10–60, MSPSf-15–60, MSPSf-20–60, and MSPSf-25–60 are 42.2, 49.6, 67.3, 78.0, 86.2, and 105.8 nm, respectively. The existence of hydrophilic SPSf, which migrates automatically to the membrane top surface thereby increasing the roughness of membrane, can explain this phenomenon. In addition, the agglomerating of SPSf at high loadings increases the hydrophilicity of membranes, which is also showing no difference in section 3.6 (pore size and porosity). This signal indicates that it is beneficial for the improvement of flux as a result of an increase in the effective membrane area caused by the nodular shapes with ridges and valleys [30].

3.6. Pore size and porosity

The bulk porosity, average pore size (r_m), and maximum pore size (r_{max}) of the PES/SPSf membrane are ranked

in Table 3, in which sulfonation degree of SPSf and water bath temperatures are varied. For membranes prepared by RTIPS method (MSPSf-0–60, MSPSf-5–60, MSPSf-10–60, MSPSf-15–60, MSPSf-20–60, and MSPSf-25–60), the porosity has a tendency to increase first and then decrease with increasing sulfonation degree of SPSf. The maximum and minimum porosity are obtained from MSPSf-15–60 and MSPSf-0–60, respectively. As for MSPSf-0–25, MSPSf-0–60, MSPSf-15–25, and MSPSf-15–60, the bulk porosity of membranes prepared by NIPS method (MSPSf-0–25, MSPSf-15–25) is lower than MSPSf-0–60 and MSPSf-15–60 prepared by RTIPS method, which is attributed to the advantage of the homogeneous porous surface by RTIPS method.

In the meanwhile, the average pore size (r_m) and maximum pore size (r_{max}) of MSPSf-0–25 and MSPSf-15–25 prepared by NIPS method are obtained the smallest values among all the membranes. These data are matched with the pure water flux and BSA rejection in Fig. 12. When the sulfonation degree of SPSf is higher than 15%, the r_m and r_{max} show a decreasing trend but still higher than the blending membrane with lower sulfonation degree, this can be explained by the increased viscosity as mentioned before.

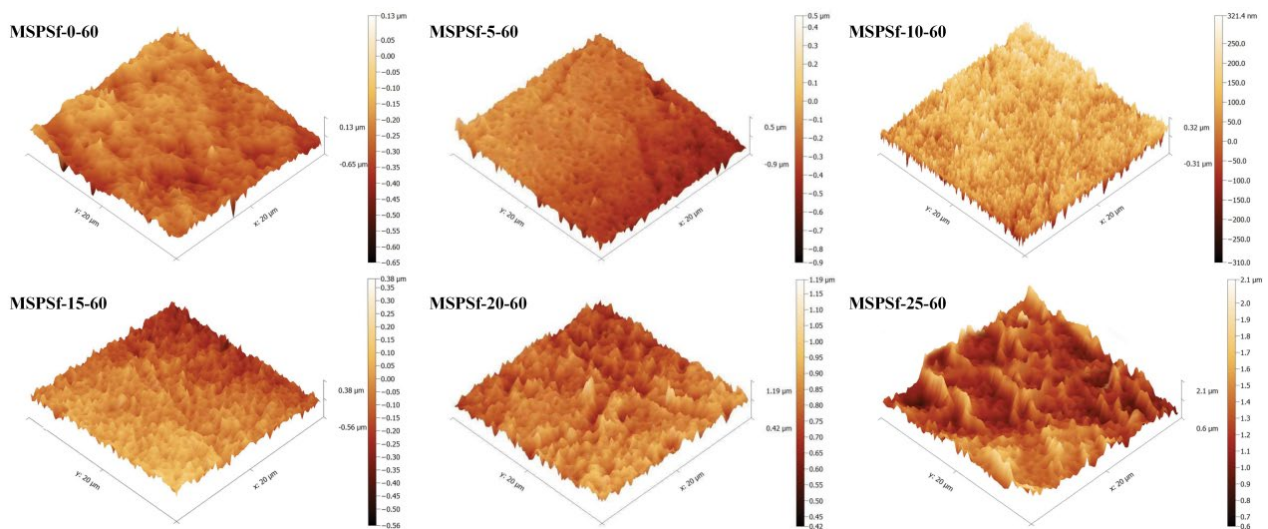


Fig. 9. AFM images of the PES/SPSf membrane.

3.7. Hydrophilicity and thermal stability of the PES/SPSf membrane

Fig. 10 shows that upon the addition of sulfonation degree of SPSf, the static pure water contact angle decreases from 91.8° for PES membrane (MSPSf-0–60) to 60.4° for the PES/SPSf membrane (MSPSf-25–60). This is entirely in agreement with those reported by others that the smaller the contact angle, the better the hydrophilicity of membranes [31–33].

The thermal stability of the PES/SPSf membrane was measured with TGA under nitrogen atmosphere as illustrated in Fig. 11. Table 4 lists the onset decomposition temperature Td^{on} and peak decomposition temperature Td^{peak} [34]. It shows that the PES/SPSf membrane displays a major weight mass loss stage at approximately 490°C owing to the fracture of PES and SPSf chains. Obviously, Td^{on} and Td^{peak} change with increasing sulfonation degree of SPSf and obtain the maximum value at MSPSf-15–60. However, the PES/SPSf membranes have a good thermal stability because the Td^{on} and Td^{peak} are higher than 477°C and 559°C, respectively, which are greatly higher than the daily use temperature of membranes.

3.8. Permeation performance

The influence of SPSf with different sulfonation degree and membrane formation mechanism on the permeation properties is shown in Figs. 12 and 13, respectively. T25 and T60 in the figures are the water bath temperature and they represent membrane formation mechanism are NIPS and RTIPS process, respectively. As illustrated in Fig. 12, pure water flux (J_w) first increase and then decrease with

increasing sulfonation degree of SPSf while BSA rejection rate shows the opposite trend. Surprisingly, the pure water flux of MSPSf-15–60 membrane (2,119 L/m² h) is as 4.2 times as that of MSPSf-0–60 membrane (510 L/m² h) in spite of the fact that its BSA rejection rate reaches 70.11%, which is not much different from other BSA rejection rates. These phenomena are matched with average pore size (r_m) in Table 3. It is because of homogeneous porous surface and spongy like cross-section obtained by RTIPS method that the pure water fluxes of all the PES/SPSf membranes are higher than that of pure PES membrane while BSA rejection rates decrease slightly.

As shown in Figs. 13a and b, the pure water fluxes (J_w) of the membranes prepared by RTIPS process (MSPSf-0–60, MSPSf-15–60) are much higher than that of NIPS process (MSPSf-0–25, MSPSf-15–25) but BSA rejection rate of MSPSf-15–60 is smaller than that of MSPSf-15–25. This is inconsistent with the advantages of the RTIPS method. In reality, MSPSf-15–60 with spongy like cross-section structure was prepared (Fig. 8), however, high average pore size (r_m) and bulk porosity of MSPSf-15–60 result in low rejection rate, therefore, the MSPSf-15–60 shows higher apparent pure water flux but lower BSA rejection rate.

Based on these phenomena, RTIPS mechanism and SPSf with different sulfonation degree have potential for obtaining blended PES membranes with good permeation performance and BSA rejection rate.

3.9. Antifouling properties

In Fig. 14a, it can be seen that membrane flux variation has a relatively smooth curve during the pure water filtration stage, then decreases suddenly during the initial

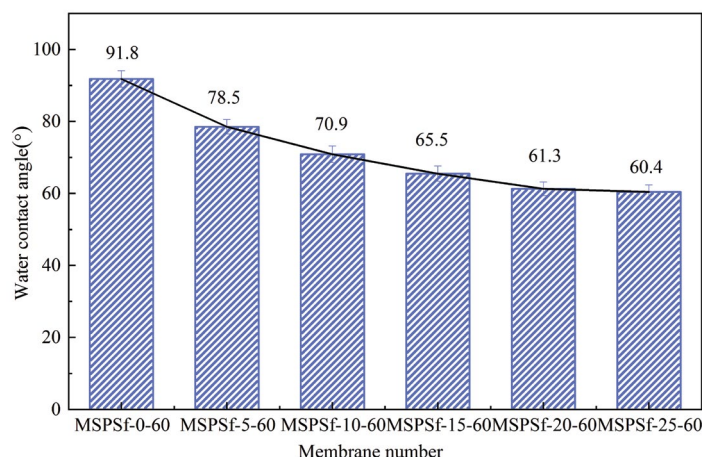


Fig. 10. Water contact angle of the PES/SPSf membrane.

Table 4
Thermal decomposition temperatures of PES/SPSf membranes

Membrane number	MSPSf-0–60	MSPSf-5–60	MSPSf-15–60	MSPSf-25–60
Td^{on} (°C)	501.8	490.6	494.4	477.2
Td^{peak} (°C)	576.9	559.4	563.8	561.0

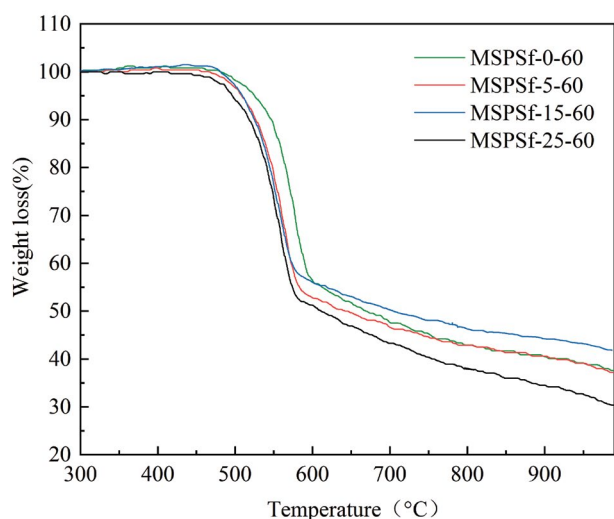


Fig. 11. TGA curves of the PES/SPSf membranes.

fouling stage. For example, the initial pure water flux of MSPSF-15-60 declines from 2,145 to 1,881 to 1,777 L/m² h after the last two pure water filtration stages. In order to observe the change of membrane fouling with time, BSA flux declines slowly with increasing sulfonation degree of SPSf, MSPSF-0-60 declines from 132 to 55 L/m² h but MSPSF-25-60 declines from 260 to 205 L/m² h, this implies the improvement of the anti-pollution performance of membranes. In addition, it is well-known that the flux recovery ratio (FRR) is used to measure membrane antifouling property, higher FRR means better anti-pollution performance. As shown in Fig. 14b, the FRR values of MSPSF-5-60, MSPSF-15-60, and MSPSF-25-60 increase with ascending sulfonation degree and they are much higher (>80%) than that of MSPSF-0-60 (59.21%). These results show that MSPSF-25-60 has the best antifouling property. Furthermore, Fig. 16 vividly shows the whole process of membrane fouling.

In sum, it is because of the hydrophilic groups brought by SPSf that the anti-pollution performance of the membrane

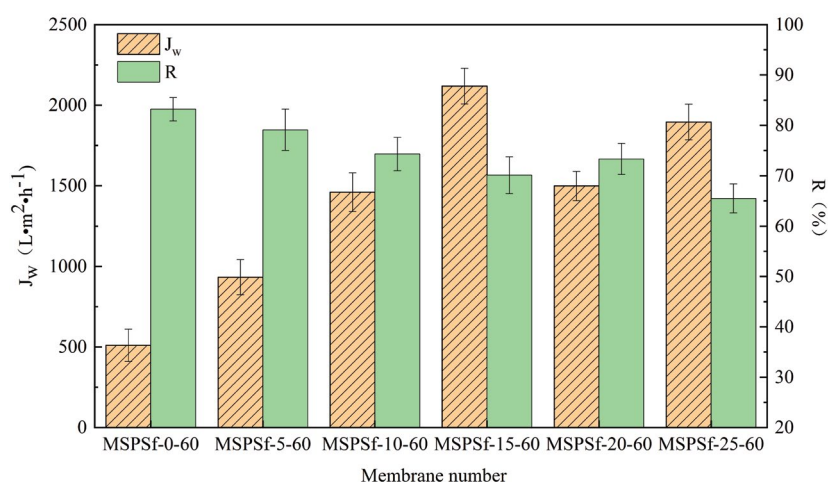


Fig. 12. Pure water flux and BSA rejection rate of the PES/SPSf membrane.

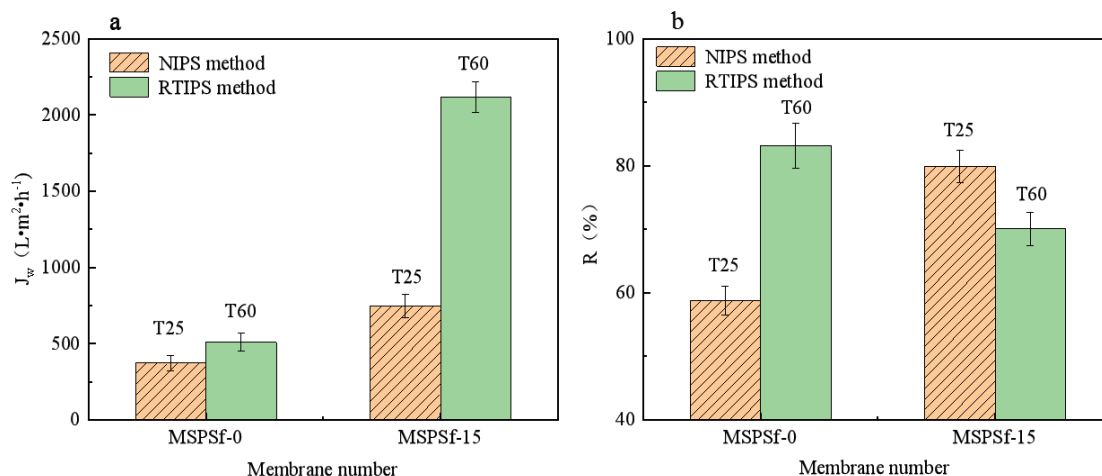


Fig. 13. (a) Pure water flux comparison of NIPS and RTIPS and (b) BSA rejection rate comparison of NIPS and RTIPS.

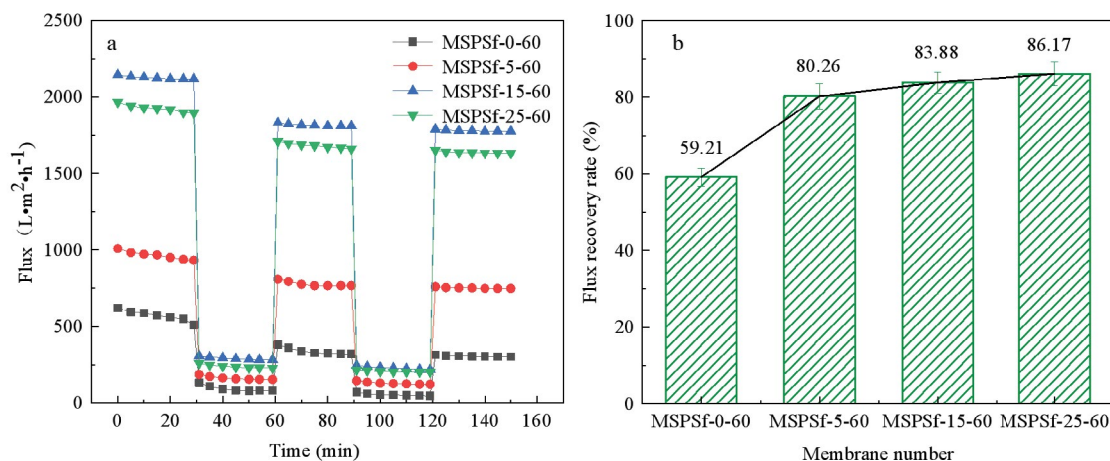


Fig. 14. (a) Flux variation of membranes during pure water and BSA fouling stage and (b) flux recovery ratio of membranes.

is improved. The highly hydrophilic sulfonic acid groups ($-\text{SO}_3\text{H}$) formed a hydration layer on the top surface of the PES/SPSf membrane and weakened the interaction between the BSA and the membrane surface, thereby hindering the fouling phenomenon of protein molecules [35], which is consistent with other studies.

3.10. Comparison with other flat-sheet membranes

The comparison of performance between this study and other flat-sheet membranes which reported in other studies [6,11,19,29,36–38] is presented in Fig. 17. High water flux and BSA rejection rate can be obtained by RTIPS method. It is attributed to sponge-like cross-section as well as homogeneous porous top surface. Moreover, the permeation performance and anti-fouling property are enhanced by increasing sulfonation degree of SPSf.

4. Conclusion

PES/SPSf membranes were prepared from PES/SPSf/DMAc/DEG casting solution with water as coagulant via NIPS and RTIPS methods. All the PES/SPSf membranes showed high decomposition temperature, which meant great thermal stability. With increasing sulfonation degree of SPSf, the static pure water contact angle decreased from 91.8° to 60.4° owing to SPSf migrated automatically to the membrane top surface thereby increasing the hydrophilicity of PES/SPSf membrane. Additionally, the pure water flux (J_w) first increased and then decreased while BSA rejection rate (R) showed the opposite trend, the maximum pure water flux obtained from MSPSf-15–60 ($2,119 \text{ L/m}^2 \text{ h}$) but the BSA rejection rate could still be kept at a high level (70.11%). Furthermore, the water FRR of membranes containing SPSf were much higher (>80%) than that of the pure PES membrane (59.21%). These results indicated that the permeability and anti-pollution performance of the PES/SPSf membrane could be enhanced with increasing sulfonation degree of SPSf.

Cloud point was used to determine the phase separation temperature. When the temperature of the water bath was higher than the cloud point, the membrane formation

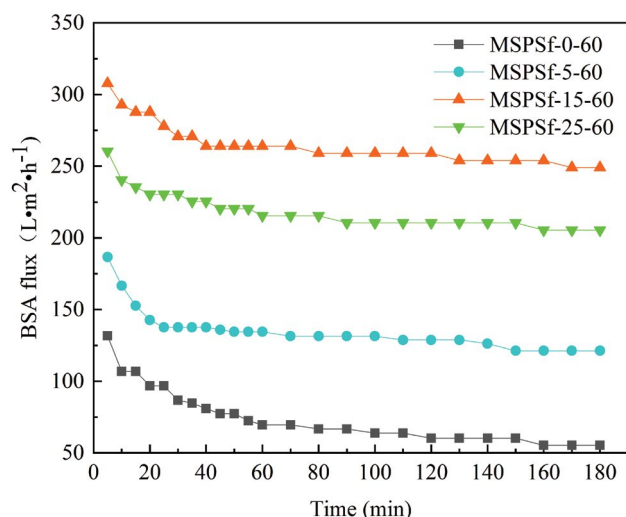


Fig. 15. Change of BSA flux with time.

process was RTIPS process. When the temperature of the water bath was lower than the cloud point, the membrane formation process was NIPS process. The dense skin surface changed into the homogeneous porous top surface as well as finger-like cross-section changed into sponge-like cross-section when the mechanism of membrane formation turned NIPS process into RTIPS procedure. In addition, pure water flux and BSA rejection rate of most membranes fabricated via RTIPS method were higher than that of NIPS method. Moreover, porosity and average effective pore size of the membranes by RTIPS also increased a lot compared with the membranes by NIPS method.

In sum, PES/SPSf membranes with different sulfonation degree of SPSf prepared via RTIPS method showed superior permeation performance and anti-pollution property.

Acknowledgments

The authors are thankful for the financial support from the National Natural Science Foundation of China (21306044),

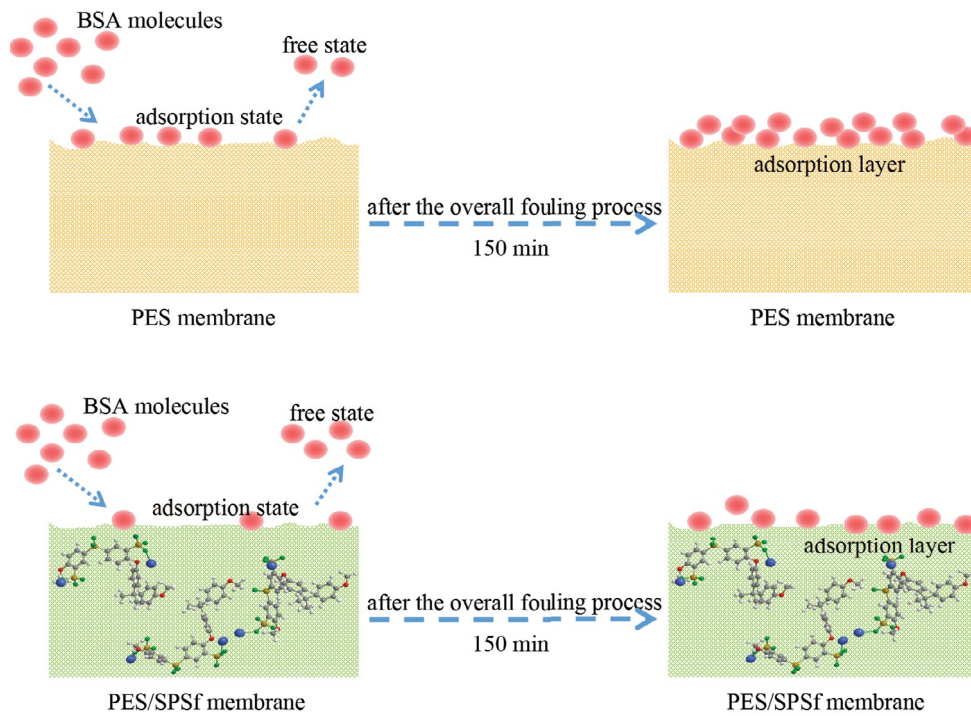


Fig. 16. Schematic diagram of the overall fouling process.

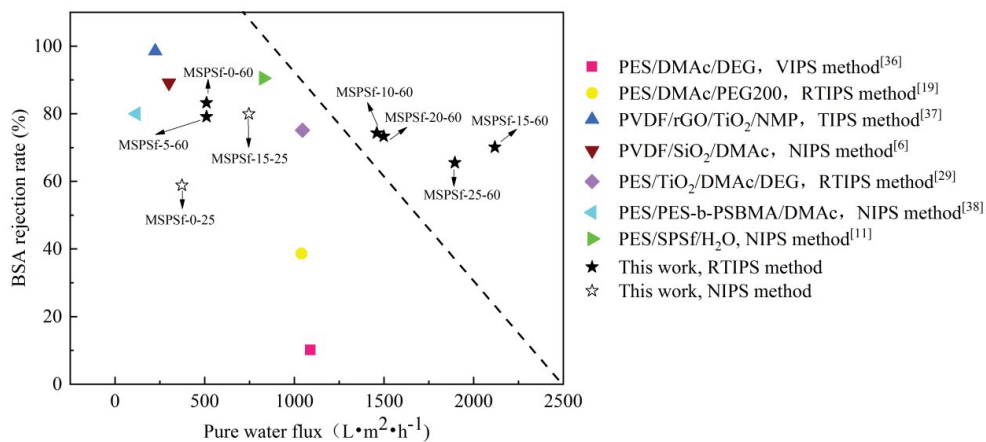


Fig. 17. Graphical representation of flat-sheet membranes performance.

China Postdoctoral Science Foundation (2015M571507), the National Science and Technology Support Project of China (2014BAB07B01 and 2015BAB09B01), the Key Technology R&D Program of Jiangsu Committee of Science and Technology in China (BE2013031), and Project of National Energy Administration of China (2011–1635 and 2013–117).

References

[1] S.W. Li, Z.Y. Cui, L. Zhang, B.Q. He, J.X. Li, The effect of sulfonated polysulfone on the compatibility and structure of polyethersulfone-based blend membranes, *J. Membr. Sci.*, 513 (2016) 1–11.
 [2] B.K. Chaturvedi, A.K. Ghosh, V. Ramachandhran, M.K. Trivedi, M.S. Hanra, B.M. Misra, Preparation, characterization and

performance of polyethersulfone ultrafiltration membranes, *Desalination*, 133 (2001) 31–40.
 [3] Y.J. Jo, E.Y. Choi, S.W. Kim, C.K. Kim, Fabrication and characterization of a novel polyethersulfone/aminated polyethersulfone ultrafiltration membrane assembled with zinc oxide nanoparticles, *Polymers*, 87 (2016) 290–299.
 [4] C. Manea, M. Mulder, Characterization of polymer blends of polyethersulfone/sulfonated polysulfone and polyethersulfone/sulfonated polyetheretherketone for direct methanol fuel cell applications, *J. Membr. Sci.*, 206 (2002) 443–453.
 [5] S.J. Oh, N. Kim, Y.T. Lee, Preparation and characterization of PVDF/TiO₂ organic-inorganic composite membranes for fouling resistance improvement, *J. Membr. Sci.*, 345 (2009) 13–20.
 [6] L.Y. Yu, Z.L. Xu, H.M. Shen, H. Yang, Preparation and characterization of PVDF-SiO₂ composite hollow fiber UF membrane by sol-gel method, *J. Membr. Sci.*, 337 (2009) 257–265.

- [7] L.J. Zhu, L.P. Zhu, J.H. Jiang, Z. Yi, Y.F. Zhao, B.K. Zhu, Y.Y. Xu, Hydrophilic and anti-fouling polyethersulfone ultrafiltration membranes with poly(2-hydroxyethylmethacrylate) grafted silica nanoparticles as additive, *J. Membr. Sci.*, 451 (2014) 157–168.
- [8] N.N. Gumbia, M.Y. Hu, B.B. Mamba, J.X. Li, E.N. Nxumalo, Macrovoid-free PES/SPSf/O-MWCNT ultrafiltration membranes with improved mechanical strength, antifouling and antibacterial properties, *J. Membr. Sci.*, 566 (2018) 288–300.
- [9] N. Nasrollahi, S. Aber, V. Vatanpour, N.-M. Mahmoodi, Development of hydrophilic microporous PES ultrafiltration membrane containing CuO nanoparticles with improved antifouling and separation performance, *Mater. Chem. Phys.*, 222 (2019) 338–350.
- [10] N. Widjojo, T.S. Chung, M. Weber, C. Maletzko, V. Warzelhan, A sulfonated polyphenylenesulfone (sPPSU) as the supporting substrate in thin film composite (TFC) membranes with enhanced performance for forward osmosis (FO), *Chem. Eng. J.*, 220 (2013) 15–23.
- [11] L. Zhang, Z. Cui, M. Hu, Y. Mo, S. Li, B. He, J. Li, Preparation of PES/SPSf blend ultrafiltration membranes with high performance via H₂O-induced gelation phase separation, *J. Membr. Sci.*, 540 (2017) 136–145.
- [12] Z.H. Sun, F.S. Chen, Hydrophilicity and antifouling property of membrane materials from cellulose acetate/polyethersulfone in DMAc, *Int. J. Biol. Macromol.*, 91 (2016) 143–150.
- [13] L.F. Fang, H.Y. Yang, L. Cheng, N. Kato, S. Jeon, R. Takagi, H. Matsuyama, Effect of molecular weight of sulfonated poly(ether sulfone) (SPES) on the mechanical strength and antifouling properties of poly(ether sulfone)/SPES blend membranes, *Ind. Eng. Chem. Res.*, 56 (2017) 11302–11311.
- [14] S.S. Madaeni, L. Bakhtiari, Thermodynamic-based predictions of membrane morphology in water/dimethylsulfoxide/polyethersulfone systems, *Polymers*, 53 (2012) 4481–4488.
- [15] A.J. Castro, Methods for Making Microporous Products, United States Patent, 4247498, 1981.
- [16] H. Matsuyama, Y. Takida, T. Maki, M. Teramoto, Preparation of porous membrane by combined use of thermally induced phase separation and immersion precipitation, *Polymers*, 43 (2002) 5243–5248.
- [17] X.F. Li, Y.G. Wang, X.L. Lu, C.F. Xiao, Morphology changes of polyvinylidene fluoride membrane under different phase separation mechanisms, *J. Membr. Sci.*, 320 (2008) 477–482.
- [18] B.J. Cha, J.M. Yang, Preparation of poly(vinylidene fluoride) hollow fiber membranes for microfiltration using modified TIPS process, *J. Membr. Sci.*, 29 (2007) 191–198.
- [19] M. Liu, Y.M. Wei, Z.L. Xu, R.Q. Guo, L.B. Zhao, Preparation and characterization of polyethersulfone microporous membrane via thermally induced phase separation with low critical solution temperature system, *J. Membr. Sci.*, 437 (2013) 169–178.
- [20] J.F. Li, Z.L. Xu, H. Yang, Microporous polyethersulfone membranes prepared under the combined precipitation conditions with non-solvent additives, *Polym. Adv. Technol.*, 19 (2008) 251–257.
- [21] M. Liu, S.H. Liu, A.L. Skov, Z.L. Xu, Estimation of phase separation temperatures for polyethersulfone/solvent/non-solvent systems in RTIPS and membrane properties, *J. Membr. Sci.*, 556 (2018) 329–341.
- [22] Y.J. Wang, D. Kim, Crystallinity, morphology, mechanical properties and conductivity study of *in situ* formed PVDF/LiClO₄/TiO₂ nanocomposite polymer electrolytes, *Electrochim. Acta*, 52 (2007) 3181–3189.
- [23] C.S. Feng, B.L. Shi, G.M. Li, Y.L. Wu, Preparation and properties of microporous membrane from poly(vinylidene fluoride-co-tetrafluoroethylene) (F2.4) for membrane distillation, *J. Membr. Sci.*, 237 (2004) 15–24.
- [24] J.F. Li, Z.L. Xu, H. Yang, C.P. Feng, J.H. Shi, Hydrophilic microporous PES membranes prepared by PES/PEG/DMAc casting solution, *J. Appl. Polym. Sci.*, 107 (2008) 4100–4108.
- [25] W.Z. Lang, Z.L. Xu, H. Yang, W. Tong, Preparation and characterization of PVDF-PFSA blend hollow fiber UF membrane, *J. Membr. Sci.*, 288 (2007) 123–131.
- [26] W.R. Bowen, T.A. Doneva, H.B. Yin, Polysulfone-sulfonated poly(ether ether) ketone blend membranes: systematic synthesis and characterization, *J. Membr. Sci.*, 181 (2001) 253–263.
- [27] Y.N. Yang, J. Wu, Q.Z. Zheng, X.S. Chen, H.X. Zhang, The research of rheology and thermodynamics of organic-inorganic hybrid membrane during the membrane formation, *J. Membr. Sci.*, 311 (2008) 200–207.
- [28] S.H. Liu, H. Yang, S.F. Ji, C.M. Gao, H. Fang, Y.Q. Xing, N.X. Han, G.D. Ding, L. Jia, Fabricating the PES/SPSf membrane via reverse thermally induced phase separation (RTIPS) process to enhance permeability and hydrophilicity, *RSC Adv.*, 9 (2019), doi: 10.1039/c9ra05707b.
- [29] S.H. Liu, M. Liu, Z.L. Xu, Y.M. Wei, X. Guo, A novel PES-TiO₂ hollow fiber hybrid membrane prepared via sol-gel process assisted reverse thermally induced phase separation (RTIPS) method, *J. Membr. Sci.*, 528 (2017) 303–315.
- [30] O. Mahlangu, R. Nackaerts, J. Thwala, B. Mamba, A. Verliefe, Hydrophilic fouling-resistant GO-ZnO/PES membranes for wastewater reclamation, *J. Membr. Sci.*, 524 (2017) 43–55.
- [31] M. Kumar, M. Ulbricht, Low fouling negatively charged hybrid ultrafiltration membranes for protein separation from sulfonated poly(arylene ether sulfone) block copolymer and functionalized multiwalled carbon nanotubes, *Sep. Purif. Technol.*, 127 (2014) 181–191.
- [32] M. Kumar, M. Ulbricht, Novel antifouling positively charged hybrid ultrafiltration membranes for protein separation based on blends of carboxylated carbon nanotubes and aminated poly(arylene ether sulfone), *J. Membr. Sci.*, 448 (2013) 62–73.
- [33] H. Susanto, M. Ulbricht, Characteristics, performance and stability of polyethersulfone ultrafiltration membranes prepared by phase separation method using different macromolecular additives, *J. Membr. Sci.*, 327 (2009) 125–135.
- [34] M. Liu, A.L. Skov, S.H. Liu, L.Y. Yu, Z.L. Xu, A facile way to prepare hydrophilic homogeneous PES hollow fiber membrane via non-solvent assisted reverse thermally induced phase separation (RTIPS) method, *Polymers*, 11 (2019), doi: 10.3390/polym11020269.
- [35] Y.H. Zhao, K.H. Wee, R. Bai, High hydrophilic and low-protein-fouling polypropylene membrane prepared by surface modification with sulfobetaine-based zwitterionic polymer through a combined surface polymerization method, *J. Membr. Sci.*, 362 (2010) 326–333.
- [36] G.E. Chen, J.F. Li, L.F. Han, Z.L. Xu, L.Y. Yu, Preparation of micro-porous polyethersulphone hollow fibre membranes using non-solvent vapour-induced phase separation, *Iran. Polym. J.*, 19 (2010) 863–873.
- [37] M. Safarpour, A. Khataee, V. Vatanpour, Preparation of a novel polyvinylidene fluoride (PVDF) ultrafiltration membrane modified with reduced graphene oxide/titanium dioxide (TiO₂) nanocomposite with enhanced hydrophilicity and antifouling properties, *Ind. Eng. Chem. Res.*, 34 (2014) 13370–13382.
- [38] Y.F. Zhao, P.B. Zhang, J. Sun, C.J. Liu, L.P. Zhu, Y.Y. Xu, Electrolyte-responsive polyethersulfone membranes with zwitterionic polyethersulfone-based copolymers as additive, *J. Membr. Sci.*, 510 (2016) 306–313.